Forward modeling by a Fourier method

Dan D. Kosloff* and Edip Baysal‡

ABSTRACT

A Fourier or pseudospectral forward-modeling algorithm for solving the two-dimensional acoustic wave equation is presented. The method utilizes a spatial numerical grid to calculate spatial derivatives by the fast Fourier transform. Time derivatives which appear in the wave equation are calculated by second-order differencing. The scheme requires fewer grid points than finite-difference methods to achieve the same accuracy. It is therefore believed that the Fourier method will prove more efficient than finite-difference methods, especially when dealing with three-dimensional models.

The Fourier forward-modeling method was tested against two problems, a single-layer problem with a known analytic solution and a wedge problem which was also tested by physical modeling. The numerical results agreed with both the analytic and physical model results. Furthermore, the numerical model facilitates the explanation of certain events on the time section of the physical model which otherwise could not easily be taken into account.

INTRODUCTION

Forward modeling by construction of synthetic data can be very useful in the interpretation of seismic time sections. In this kind of work, synthetic data are compared to field results to determine how the assumed geologic model of the subsurface needs to be modified to obtain better agreement between calculations and observations.

Two important techniques which have been used for forward modeling are the finite-difference method and the finite-element method. Both methods can account for complex geologic structures and can handle the elastic wave equation. Their main drawback has been a practical limitation on high-frequency resolution. The rule of thumb often used in this context has been that ten grid points (elements) are required to resolve a given wavelength (Alford et al, 1974). For typical wave velocities and frequency bands encountered in exploration seismology, this rule can imply grid-point spacings on the order of 3–4 m. It is therefore apparent that realistic geologic problems require a very large number of grid points, especially in three dimensions (3-D) thus entailing prohibitive amounts of computer time.

This study examines forward modeling in two dimensions (2-D) by the Fourier method or, as it is often called, the pseudospectral method (Kreiss and Oliger, 1972; Fornberg, 1975, 1977; Orzag, 1980; Gazdag, 1981). This method differs from the finite-difference technique in that it uses the fast Fourier transform (FFT) for calculating spatial derivatives instead of finite differences. The resulting derivative operators are highly accurate, and our results as well as those of others (Fornberg, 1975; Gazdag, 1981) indicate that only two grid points are required to resolve a spatial wavelength. Thus, compared to finite differences or finite elements, the Fourier method requires a factor of 25 fewer grid points in 2-D and 125 fewer in 3-D for achieving the same accuracy. For this reason we believe the Fourier method can considerably improve forward modeling and, at least in 2-D, enable one to model in the full frequency band used in exploration geophysics.

In the following sections we describe the algorithm which was constructed for solving the 2-D acoustic wave equation and present two examples which shed light on some features of the Fourier method and its possible application.

THE SOLUTION ALGORITHM FOR THE ACOUSTIC WAVE EQUATION

When both density and seismic wave velocity are spatially variable, the acoustic wave equation reads

$$\frac{\partial}{\partial x}\left(\frac{1}{\rho}\frac{\partial P}{\partial x}\right) + \frac{\partial}{\partial y}\left(\frac{1}{\rho}\frac{\partial P}{\partial y}\right) = \frac{1}{c^2\rho}\ddot{P} + S, \qquad (1)$$

where $P(x, y, t)$ represents the pressure, $\rho(x, y)$ the density, $c(x, y)$ the wave velocity, and $s(x, y, t)$ the source term which equals the divergence of the body force divided by the density. In equation (1) and throughout, a dot above a variable denotes differentiation with respect to time.

The Fourier method solves equation (1) by a discretization in both space and time, yielding a discrete approximation to equation (1) given by

$$LP^n(i, j) = \frac{1}{c^2\rho\,\Delta t^2}\left[P^{n+1}(i, j) - 2P^n(i, j)\right.$$
$$\left. + P^{n-1}(i, j)\right] + S^n(i, j), \qquad (2)$$

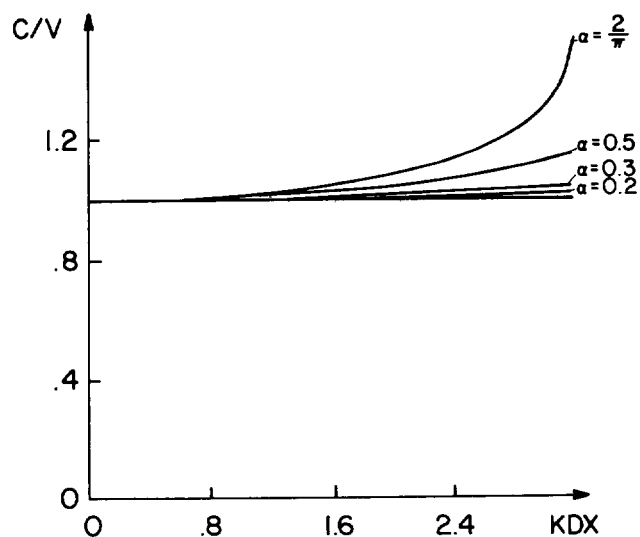where $P^n(i, j)$ and $S^n(i, j)$, respectively, represent the values of

FIG. 1. Normalized phase velocity C/V versus wavenumber $K \Delta X$ for the Fourier method for the 1-D homogeneous wave equation for different ratios of $\alpha = V\Delta t/\Delta x$, where V is the velocity of propagation.
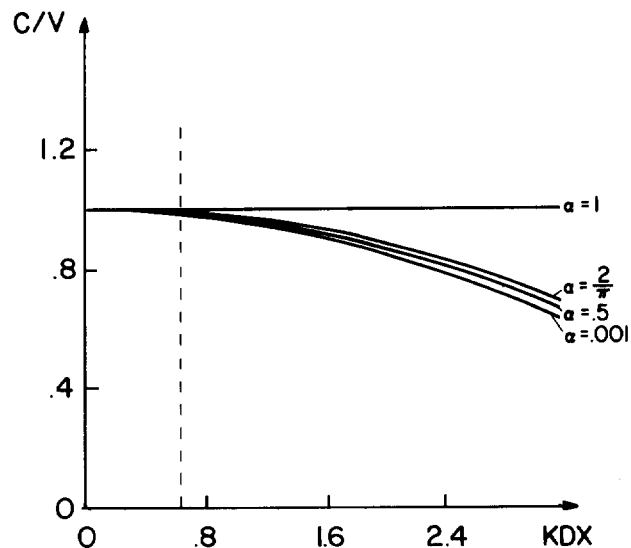

FIG. 2. Normalized phase velocity versus wavenumber for a second-order differencing scheme for the 1-D homogeneous wave equation (after Alford et al, 1974).

pressure and source at time $t = n\Delta t$ and at spatial location $x = x_0 + (i - 1)\Delta x$, $y = y_0 + (j - 1)\Delta y$. $LP''(i, j)$ represents the numerical approximation of the left-hand side of equation (1).

Equation (2) ontains an explicit, second-order, time-differencing scheme similar to schemes often used in finite-difference and finite-element codes. The point of departure for the Fourier method is the manner in which the spatial derivatives are calculated.

The term $LP''(i, j)$ in equation (2) is calculated in two separate passes, one for the terms containing x-derivatives and one for the terms containing y-derivatives. In the pass for the x-derivatives, $\partial/\partial x[(1/\rho)(\partial P/\partial x)]$ is calculated for each of the grid lines which parallels t' x-directions (hereafter referred to as x-lines). Along each x-line $\partial P/\partial x$ is calculated by first performing a spatial FFT on P. The result is then complex multiplied by the spatial wavenumber vector iK_v, $v = 1 \ldots, N_x$, where N_x is the number of grid points in each x-line and $i = \sqrt{-1}$. This operation is followed by an inverse FFT into the spatial domain yielding $\partial P/\partial x$. In the second stage, $\partial P/\partial x$ is multiplied by the vector $1/\rho$, and again a forward and inverse FFT are used to get $\partial/\partial x[(1/\rho)(\partial P/\partial x)]$. When the calculation has been completed along all the x-lines, a similar process is applied in a second pass to get $\partial/\partial y[(1/\rho)(\partial P/\partial y)]$ along all the y-lines.

FEATURES OF THE FOURIER METHOD

Spatial derivatives constructed by the Fourier method are infinitely accurate for pressures with spatial frequencies in the band of the mesh. For a problem in an infinite homogeneous region, the Fourier components are eigenvectors of the wave equation, and the temporal frequency of the exact solution will equal the frequency band of the source term $S(x, y, t)$. In such a case, when the frequency band of the source is appropriately chosen, errors in the numerical solution come only from the inaccuracy

of the finite-difference approximation of the time derivative. These errors manifest themselves as numerical dispersion and diminish rapidly with a decrease in the size of the time step.

Figure 1 plots the dispersion relation for the Fourier method for the one-dimensional (1-D) homogeneous wave equation. In this plot C is the phase velocity and V is the acoustic wave speed. Details of the derivation of the formula on which the plot is based are given in the Appendix. The plot shows that at the stability limit when $\alpha = c\Delta t/\Delta x = 2/\pi$, the numerical dispersion is large. However, for time steps for which $\alpha < 0.2$, the dispersion will become small.

When density or velocity are spatially variable, the frequency band of the solution of the wave equation may no longer be equal to the frequency band of the source. This is because a multiplication by density or velocity in the spatial domain corresponds to a convolution in the spatial-frequency domain. Therefore not all errors in this situation can be attributed to numerical dispersion. In spite of this, our experience indicates that by using time steps for which $\alpha < 0.2$ at all grid points, and limiting the frequency content of the source to the band resolvable by the grid, one obtains crisp and clear events on the time sections. To be more cautious, the first test case which we present compares numerical results to analytic results for a single plane interface problem, and agreement proves close indeed.

Figure 2 presents for comparison the dispersion relation for a 1-D finite-difference scheme used by Alford et al (1974). The figure shows that dispersion at high frequencies is always large except at the stability limit $\alpha = 1$. The dashed line corresponds to a wavelength of ten grid points which, as stated previously, is often considered to be the shortest wavelength which can be resolved. At this wavelength the phase velocity is about 2 percent less than the acoustic wave speed.

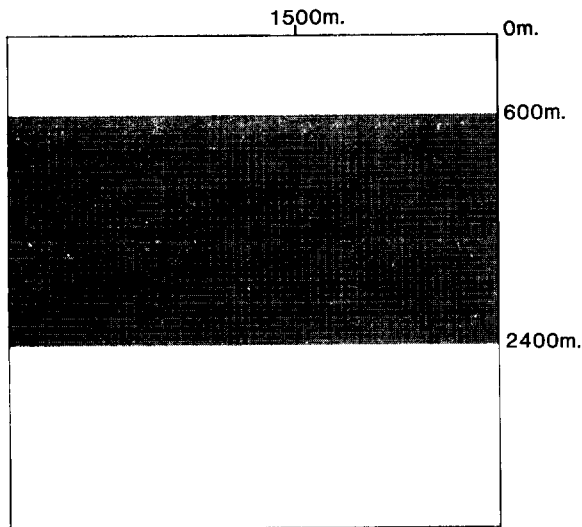An additional advantage of the Fourier method over the finite-

1500m. Om.

600m.

2400m.

FIG. 3. Model configuration for plane interface example.

pendence of the source must be carefully chosen in order to limit its frequency band to the range which can be resolved by the spatial grid. If this is not done, erroneous long-period components can enter the solution through aliasing, in a manner which cannot be easily remedied by postfiltering. The formula we adopted for the maximum source frequency is derived on the basis that in a plane harmonic wave the wavelength λ is related to the velocity c and frequency f by $\lambda = c/f$. The criterion which we used for the frequency content of the source was therefore given by

$$f_{max} = \frac{c_{min}}{2 \max (\Delta x, \Delta y)}, \tag{3}$$

where c_{min} is the lowest acoustic velocity in the region modeled, and Δx and Δy are the grid spacings in the x- and y-directions, respectively. The denominator of equation (3) is equal to the Nyquist spatial wavelength in the x- or y-directions, whichever is larger. A similar formula was derived from a different consideration for the first-order, one-way equation by Fornberg (1975).

In constructing the grid for forward modeling, one must choose a large enough grid to ensure that important events arrive before "wrap-around" events from grid boundaries. The considerations here are similar to those encountered in constructing finite-element or finite-difference grids. Wrap-around from the lower boundary can be eliminated by specifying a condition of zero pressure at the earth's surface. This, however, has the penalty of creating ghost events on the records, since the source must be placed below the first row of grid points.

Specification of the grid, the material parameters, and the source term completes the input data for the forward model. The calculations yield pressure time histories of all the grid points, which can be analyzed later by various graphic displays.

Example: A plane interface

The first example compares numerical and analytical solutions for a problem of a point source above a plane interface between two half-spaces with contrasting material properties. The model configuration is shown in Figure 3. Since the numerical mesh covers only a finite region, the lower half-space was approximated by a thick layer (shaded region in Figure 3). For times shorter than the reflection time from the bottom of the layer (and of the wrap-around reflection from the same interface), the solution of this problem should be identical to the solution of the problem of two half-spaces in contact. The bottom region of the mesh (un-
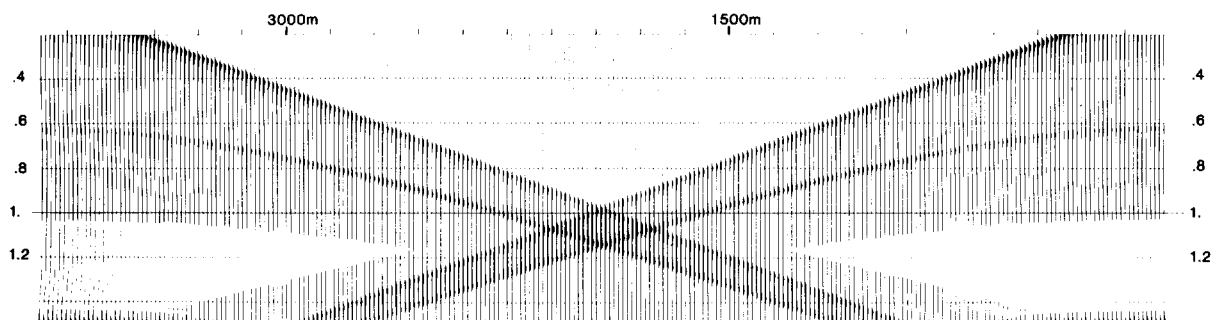
difference method is that for a 2-D or 3-D homogeneous medium the dispersion is isotropic. Thus a Fourier component of a given frequency will travel at the same phase velocity at all angles with respect to the grid. This usually is not the case with finite differences for which dispersion is often anisotropic at high frequencies (Alford et al, 1974).

INPUT DATA FOR FORWARD MODELING

In a forward model, the geologic structure and the seismic source are assumed known, and the calculations yield the pressure as a function of time and space. In the Fourier modeling method, the geologic structure is specified through the density and seismic wave velocity (or bulk modulus) at the grid points. The method allows for both continuous and discontinuous variation of the material parameters.

The source term in equation (2) is usually applied at a single point at the top of the grid to imitate a seismic shot. The time de-

3000m 1500m

.4 .4

.6 .6

.8 .8

1. 1.

1.2 1.2

FIG. 4. Time section of the top row of the mesh for the plane interface example. Times are given on the right of the figure in seconds.

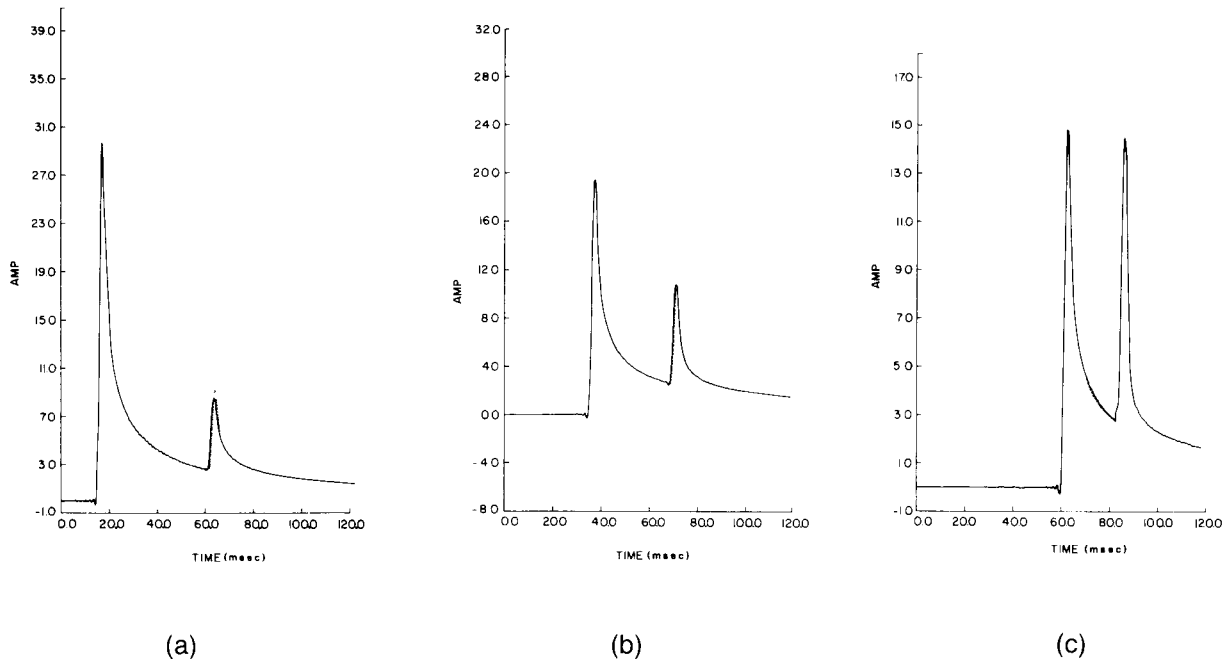(a)   (b)   (c)

FIG. 5. Comparison of numerical (solid lines) and analytical (dashed lines) pressure histories for the single-layer example for stations on the surface at respective distances from the source of 300, 750, and 1200 m.

shaded area) had the same material properties as the top half-space. Wrap-around to the lower boundary was allowed in this example because no zero-pressure boundary conditions were applied at the top of the mesh.

The material properties for this problem were a wave velocity of 2000 m/sec with a density of 2.1 g/cm^3 for the unshaded region in Figure 3, and a velocity of 4000 m/sec with a density of 2.5 g/cm^3 for the shaded region. The source was applied at the right upper corner of the mesh at a height of 600 m above the interface. It had a triangular time dependence with a half-duration of 20 msec. Most of the frequency content of this source was below 60 Hz.

The calculation used 256 × 256 mesh points with a grid spacing of 15 m. The time step was 1 msec, and the calculation was carried out to 1.5 sec or 1500 time steps. The calculation was performed on the VAX-11 computer at the Seismic Acoustics Laboratory (SAL) which is equipped with a Floating Point Systems array processor. The computations took about three hours (wall-clock time).

The time section for the upper line of the grid is shown in Figure 4. The section shows the direct and reflected arrivals. The refracted head wave is also present, but it is weak and not easily distinguished. The arrivals from the left corner are wrap-around events. For interpretation purposes, arrivals in the right half of the grid are usually considered for times shorter than the arrival time of the wrap-around events.

In order to examine the numerical scheme more closely, Figures 5a, 5b, and 5c present single trace histories at surface points

with respective distances of 300, 750, and 1200 m from the source. These distances correspond to subcritical, near-critical and postcritical reflection angles. The dashed line in each figure gives the analytic solution to the problem based on the Cagniard technique (Aki and Richards, 1980). Agreement between numerical and analytical solutions appears satisfactory.

Finally, Figures 6a, 6b, and 6c give the amplitude as a function of space at different times. In Figure 6a the cylindrical wave has developed but has not reached the layer. Wrap-around from the corners of the grid is apparent. Figure 6b gives amplitudes at $t = 0.4$ sec. The wavefront has reached the layer, and the reflected and transmitted waves are present. Figure 6c corresponds to a later time, $t = 0.7$ sec. The refracted head wave is clearly visible in this figure.

Example: A buried wedge

The buried wedge example compares experimental measurements for a physical model with numerical computations. The physical model is a silicone rubber 2-D wedge lying on a flat, level Plexiglas plate (Figure 7). The model was submerged in water. The length and time dimensions for the experimental measurements were scaled upward to correspond with typical parameters encountered in exploration geophysics. The scaled velocities for the materials were (velocity and density, respectively) 4000 m/sec and 1 g/cm^3 for the water, 2300 m/sec and 1.17 g/cm^3 for the wedge, and 6000 m/sec and 1.17 g/cm^3 for the plate. The spatial dimensions of the model are shown in Figure 7.
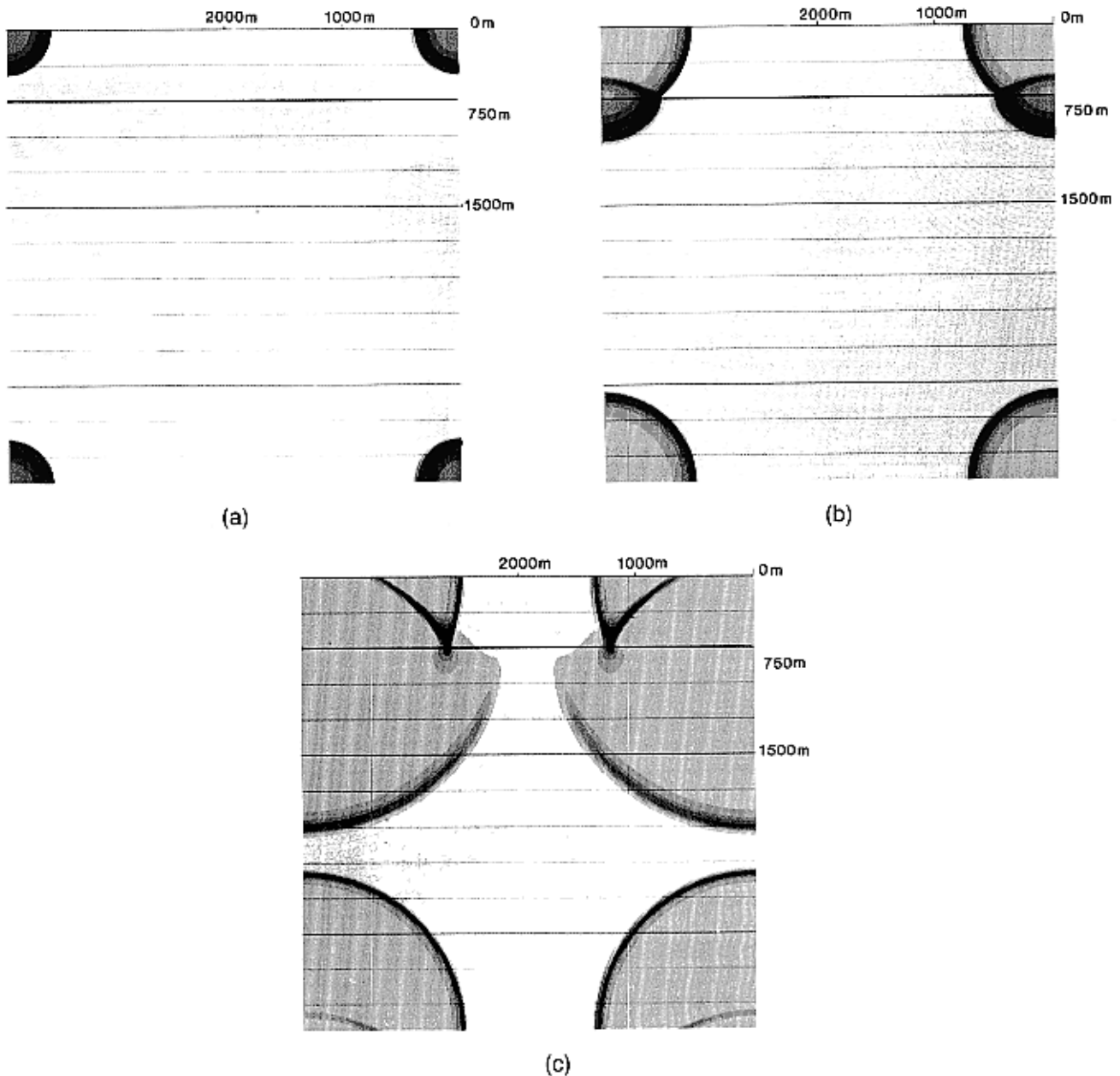
FIG. 6. Amplitude as a function of space at times (a) 0.2 sec, (b) 0.4 sec, and (c) 0.7 sec.

Figure 8 presents a single-fold, zero-offset time section for the physical model at a height of 2875 m above the Plexiglas plate, and a horizontal range between 2430 and 9170 m. The reflections from the sloping sides of the wedge are identified in Figure 8 as events A and B. Events C and D are identified as reflections from the Plexiglas plate.

There are, however, a number of features in Figure 8 which are more difficult to explain. For example, the origin of event E is not clear. Also, event C has a sloping continuation to the left of its horizontal portion, whereas event D is truncated and its continuation appears to occur later as a separate event F.

In this section we attempt to interpret event F with the aid of

numerical simulations. For this purpose, two common shot gathers are considered with shot locations at 5000 and 7500 m, respectively. The source wavelet for the simulations was a 4–40 Hz zero-phase, band-limited signal with a peak amplitude at 100 msec delay. The calculations used a mesh size of 20 m with 512 grid points in horizontal dimension and 128 points in vertical dimension. In this example, the FFTs in the vertical direction were padded with zeroes to 512 points, yielding in effect a zero-pressure boundary condition on the earth's surface. Thus all the calculated sections contain a ghost from the reflection of the surface of the earth.

Figure 9 presents the calculated common-shot gathers for a shot

location at 5000 m. In the figure, event 1 is identified as the direct wave, event 2 is the reflection from the side of the wedge (event A in Figure 8), and event 3 is the reflection off the Plexiglas plate (event C in Figure 8). For comparison, Figure 10 presents a physical model common shot gather with the same shot location. The correspondence between this figure and Figure 9 is straightforward. The differences between the figures can be attributed to slight variations between material parameters of the two models, a difference between the 2-D spreading law of the numerical simulation and the 3-D spreading law of the physical model, and a difference in the waveform and the directivity of the sources (the free-surface ghost creates a directivity pattern in the numerical simulation, and the physical model source is known to have directivity).

The main interpretive tools of the numerical simulations are the plots of amplitude in space at given times (shapshots). Figure 11 presents amplitude at time $t = .675$ sec for the shot location at 5000 m. At this time the cylindrical wave from the source impinges on the side of the wedge, developing transmitted and reflected waves. Figure 12 shows the amplitude at time $t = .975$ sec after the waves have reached the Plexiglas plate. The reflected wave from the Plexiglas is continuous across the wedge boundary (events 3 and 4, respectively). When this reflection approaches the surface at the source location (Figure 13), the reflected front maintains continuity. This explains why event C in Figure 8 is continuous, since no break occurs between waves which reach the Plexiglas directly from the water and waves which reach the Plexiglas through the wedge.

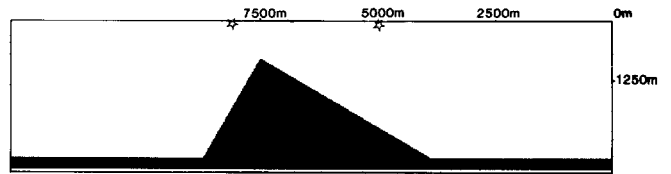For the source at 7500 m, the numerical simulation exhibits

FIG. 7. Model configuration for the wedge example.

different characteristics of reflection due to the steep dip of the left portion of the wedge. Figure 14 presents amplitude at time $t = .975$ sec soon after the generation of reflections from the Plexiglas plate. In this figure the reflection from the Plexiglas through water (event D) is separated from the reflection through the wedge (event F). In Figure 15, event D has arrived at the shot location, whereas event F is traveling in the wedge with a wavefront approximately perpendicular to the wedge-water boundary.

The absence of a continuation of event F in the water across the wedge boundary is due to the low velocity of the wedge material which causes critical reflection behavior. Event F eventually reaches the shot location as a weak corner diffraction (Figure 16). The similarity of event F on the single-fold section (Figure 8) to the sloping portion of event C is not a coincidence since the two events are essentially identical except for the separation of event F from event D due to postcritical reflection angles.
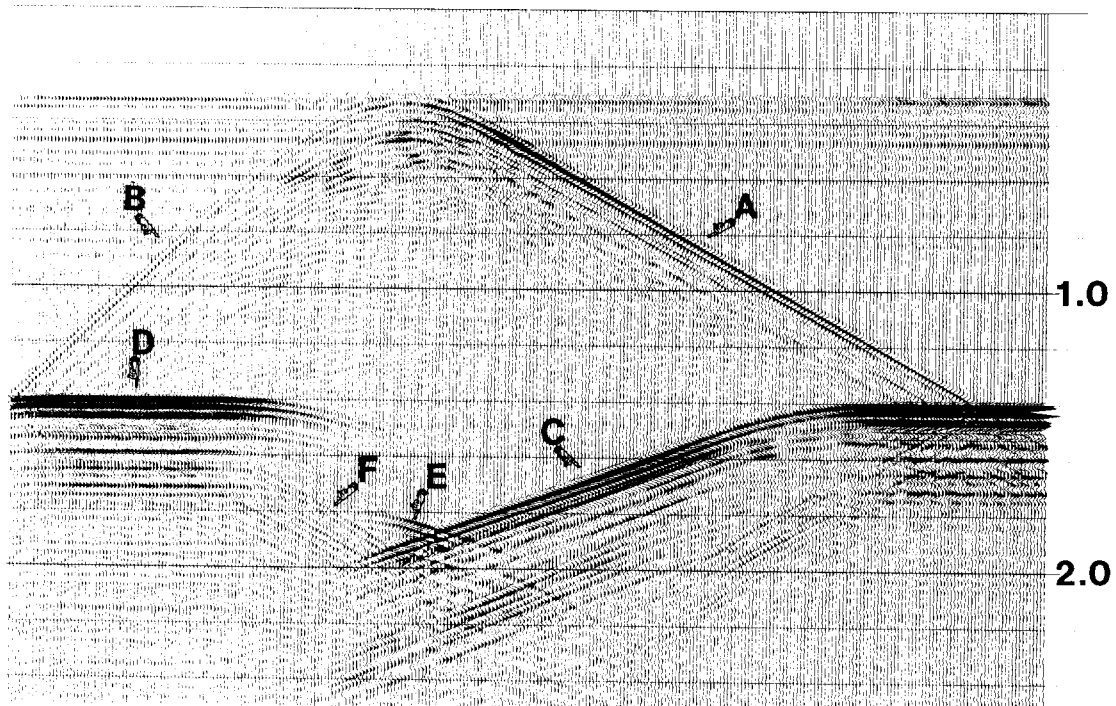

FIG. 8. Zero-offset time section for the physical model.
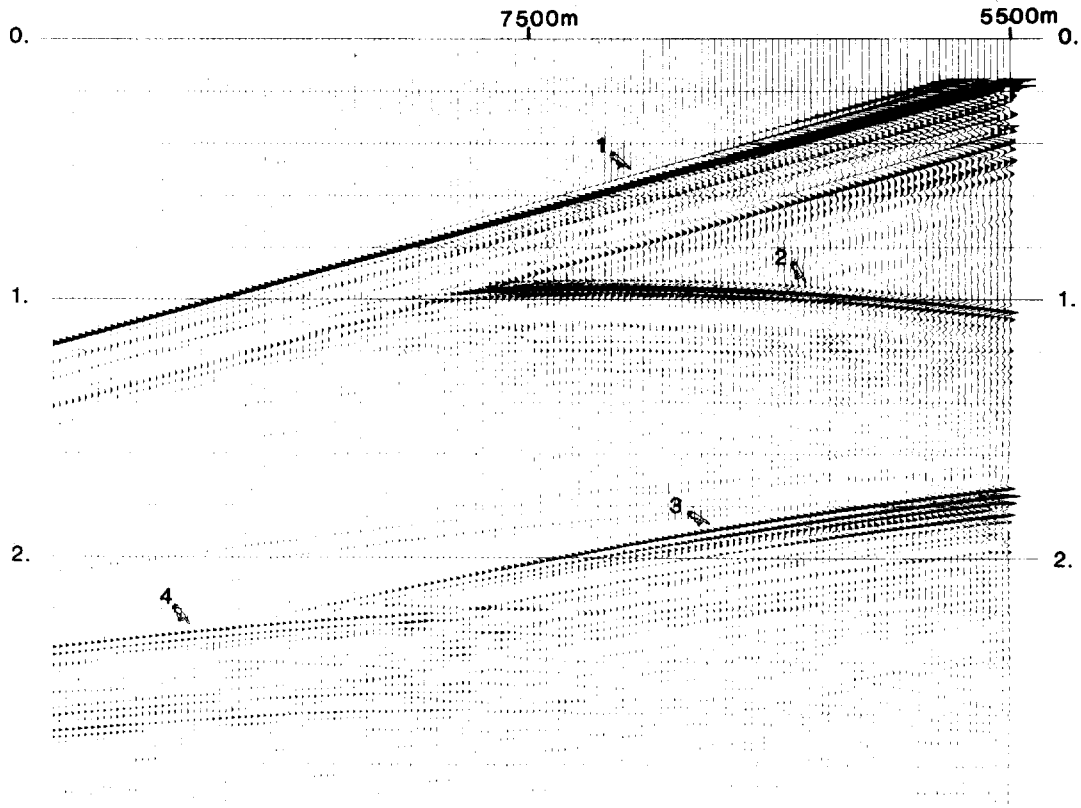
FIG. 9. Common-shot gather for the numerical model.

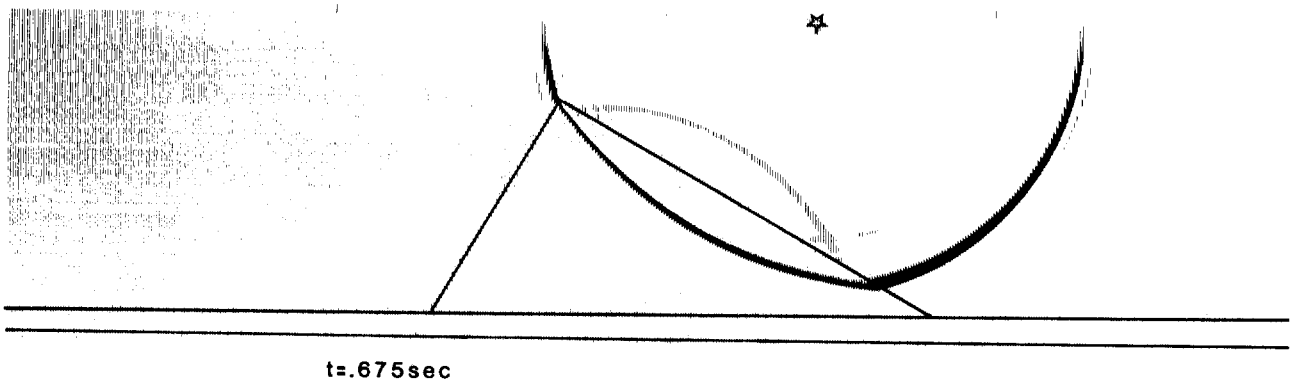FIG. 10. Common-shot gather for the physical model.

t=.675sec

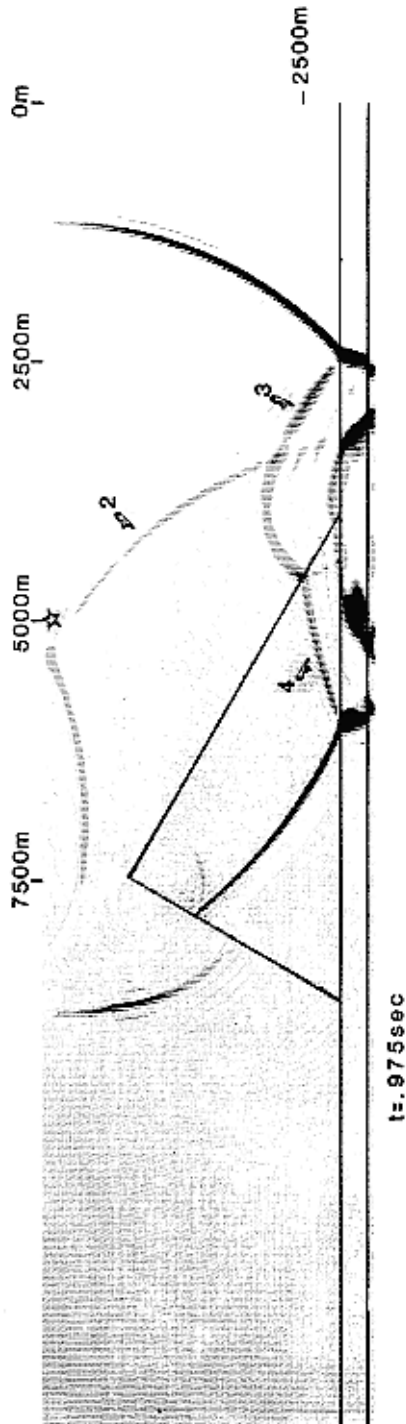FIG. 11. Amplitude at $t = .675$ sec for shot location at 5000 m.

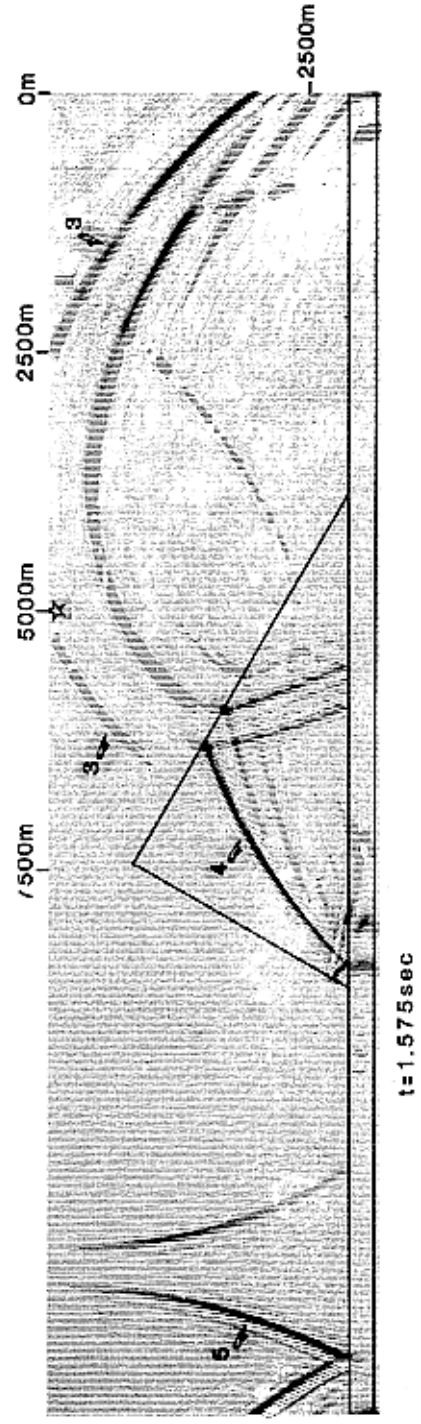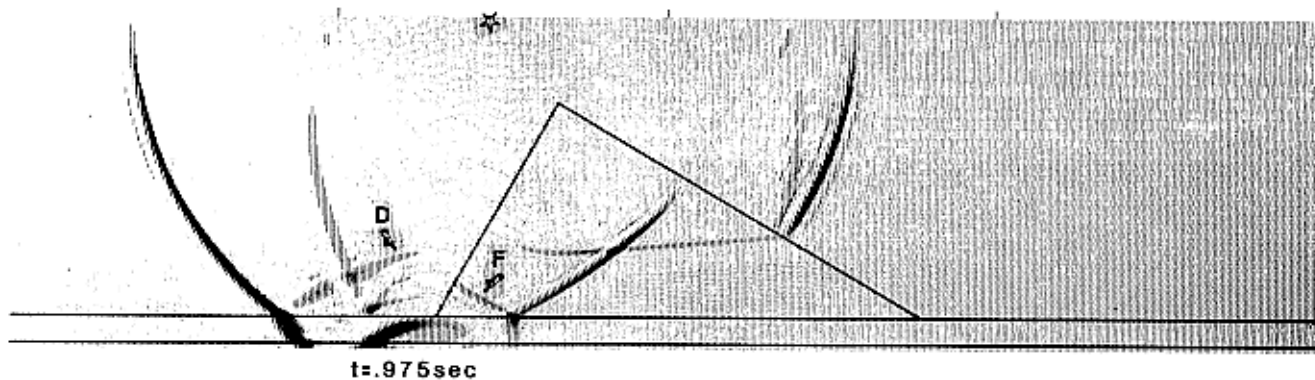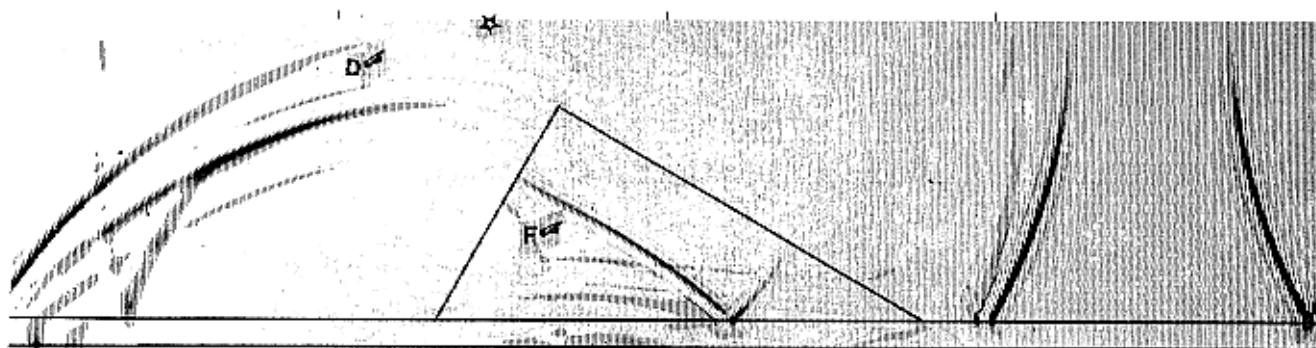FIG. 12. Amplitude at $t = .975$ sec for shot location at 5000 m.

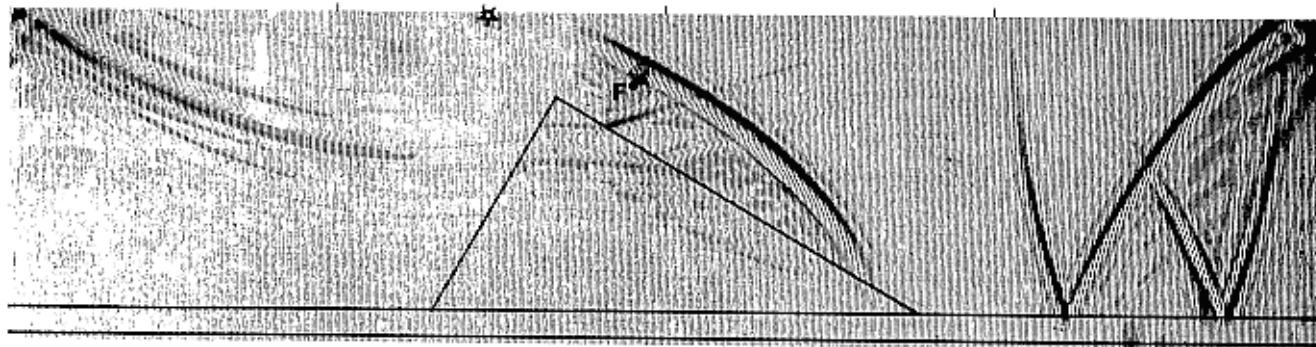FIG. 13. Amplitude at $t = 1.575$ sec for shot location at 5000 m.

FIG. 14. Amplitude at $t = .975$ sec for shot location at 7500 m.

FIG. 15. Amplitude at $t = 1.5$ sec for shot location at 7500 m.

FIG. 16. Amplitude at $t = 2.025$ sec for shot location at 7500 m.

CONCLUSIONS

A forward modeling scheme has been presented, based on a Fourier method. The scheme enables the building of models of realistic geologic structures in 2-D and calculating synthetic seismograms in the frequency band often used in exploration seismology. As with finite differences and finite elements, the capability of the scheme to produce plots of amplitude in space at specified time (snapshots) enables easy interpretation of complex events on time sections.

The Fourier method is more complicated than finite differences in that computations are not performed locally around each element of the grid, but rather along complete lines in the coordinate directions. On the other hand, the Fourier method requires fewer grid points than the finite-difference method to achieve the same resolution. We believe the savings in computation time because of the reduction in the number of grid points outweighs the added number of calculations arising from the complexity of the Fourier method. This advantage should become more apparent in 3-D where the Fourier method requires a factor of 125 fewer grid points than the finite-difference method to achieve equivalent accuracy.

REFERENCES

Aki, K., and Richards, P. G., 1980, Quantitative seismology, theory and methods: W. H. Freeman and Co., San Francisco.
Alford, R. M., Kelly, K. R., and Boore, D. M., 1974, Accuracy of finite-difference modeling of acoustic wave equations: Geophysics, v. 39, p. 834–841.
Fornberg, B., 1975, On a Fourier method for the integration of hyperbolic equations: SIAM J. Num. Anal., v. 12, p. 509–528.
———— 1977, A numerical study of 2-D turbulence: J. Comp. Phys., v. 25, p. 1–31.
Gazdag, J., 1981, Modeling of the acoustic wave equation with transform methods: Geophysics, v. 46, p. 854.
Kreiss, H. O., and Oliger, J., 1972, Comparison of accurate methods for the integration of hyperbolic equations: Tellus, v. 24, p. 199–215.
Orzag, S. A., 1980, Spectral methods for problems in complex geometries: J. Comp. Physics, v. 37, p. 70–92.

APPENDIX
DISPERSION RELATIONS FOR THE FOURIER METHOD

(1) 1-D homogeneous case

When density and bulk modulus are constant, the 1-D acoustic wave equation can be written

$$\frac{\partial^2 P}{\partial x^2} = \frac{1}{c^2} \frac{\partial^2 P}{\partial t^2}, \tag{A-1}$$

where c is the wave velocity. The second time derivative in equation (A–1) is approximated by

$$\frac{P^{n+1} - 2P^n + P^{n-1}}{\Delta t^2}$$

where $P^n = P(x, t = n\Delta t)$.

Assume a solution of equation (A–1) of the form $e^{i(kx - \omega t)}$, where the wavenumber k is in the band of the numerical mesh. With this solution the left-hand side of equation (A–1) gives $-k^2 e^{i(kx - \omega t)}$, whereas the right-hand side gives $-(1/c^2 \Delta t^2) \cdot e^{i(kx - \omega t)} \cdot 4 \sin^2 \omega \, \Delta t/2$.

By equating both sides, we get the dispersion relation,

$$\mp k = \frac{2}{c\Delta t} \sin \frac{\omega \Delta t}{2}. \tag{A-2}$$

For equation (A–2) to hold for real ω, the time step must satisfy the relation

$$c\Delta t < \frac{2}{k}, \text{ for all } k. \tag{A-3}$$

The largest k is at the Nyquist spatial frequency for which $k = \pi/\Delta x$ with Δx the grid spacing. A substitution of this value in equation (A–3) gives $c\Delta t/\Delta x < 2/\pi$ which defines the stability criterion.

(2) 2-D homogeneous case

The derivation follows the same steps as in the 1-D case. Substituting a trial solution $e^{i(k_x x + k_y y - \omega t)}$ in the discretized acoustic wave equation gives the dispersion relation

$$\sqrt{k_x^2 + k_y^2} = \frac{2}{c\Delta t} \sin \frac{\omega \Delta t}{2}. \tag{A-4}$$

For real ω, Δt must satisfy the inequality

$$c\Delta t < \frac{2}{\sqrt{k_x^2 + k_y^2}}. \tag{A-5}$$

At the Nyquist spatial frequencies in x and y and for a uniform Δd grid spacing in x and y, $k_x = \pi/\Delta d$ and $k_y = \pi/\Delta d$. For these values we obtain the 2-D stability criterion

$$c \, \Delta t/\Delta d < \sqrt{2}/\pi. \tag{A-6}$$